International Research Journal of Engineering and Technology (IRJET) e-ISSN: 2395-0056
Volume: 11 Issue: 09 | Sep 2024 www.irjet.net p-ISSN: 2395-0072

Tube Pod Interdependency for Hyperloop Optimal Aerodynamic Design

Rahul Sahu[1], Swastika Patel[1*], Prashant Kumar Sahu[2], Gulab Verma[2], Sunil Kumar Patel[1]

[1]Assistant Professor, Dept. of Mechanical Engineering, Government Engineering College, Raipur, Chhattisgarh, India PIN-492015

[2] Assistant Professor, Dept. of Mechanical Engineering, Government College of Engineering, Jagdalpur, Chhattisgarh, India PIN-494001

Abstract

Traditional modes of transportation, such as rail, road, water, and air, often exhibit limitations in terms of speed, cost, or a combination thereof. In contrast, Hyperloop emerges as a revolutionary transport mode, promising both rapid transit and cost-effectiveness for passengers and cargo. Unlike conventional systems, Hyperloop adopts an open design concept akin to Linux, featuring a low-pressure tube through which capsules travel at varying speeds. These capsules, supported by air cushioning and aerodynamic lift, are propelled by magnetic linear accelerators stationed at intervals along the tube. Hyperloop stations can be situated at tube ends or along its length, facilitating convenient passenger embarkation and disembarkation. This study delves into the feasibility of the high-speed Hyperloop system, considering factors such as high-pressure differentials, shock waves, boundary layer dynamics, blockage ratios, Kantrowitz limits, and various drag forces, including wave, pressure, and viscous drag. The project aims to determine the maximum achievable velocity of Hyperloop pods under diverse parameters such as initial velocity, tube pressure, and pod length while assessing the inherent drag forces in its operation. Utilizing computational fluid dynamics, velocity and pressure profiles along the Hyperloop length will be analyzed, providing valuable insights into its aerodynamic performance.

Keywords: Aerodynamic, Analysis, Computational, Hyperloop, Velocity.

1. Introduction

The Hyperloop is a conceptual transportation system that reduces costs and travel times compared to California's existing high-speed rail project. It was introduced as an open-source design for public review and further development by Elon Musk and a team of engineers from Tesla Motors and SpaceX in August 2013. Unlike conventional high-speed rail systems, the Hyperloop replaces rails with a tube that encloses the passenger pod in a partial vacuum and suspends it on air bearings. Propulsion is achieved using linear electromagnetic accelerators installed along the tube, with the system elevated on concrete columns to maintain a relatively straight path. Since Hyperloop operates at transonic speeds and in a low-pressure environment, the tube design becomes more vital as the air flowing over the pod length is subjected to a lower cross-sectional area. This causes air flow over the pod to accelerate, which can even reach a low supersonic range and lead to the development of shock waves.

Further, there is a continuous increase in the boundary layer thickness along the length of the hyperloop pod, i.e., a constant reduction in mass flow rate over the pod length, which may cause choked flow or can lead to boundary layer sensitivity. To treat this, there should be sufficient tube cross-sectional area to compensate for the reduction in mass flow rate. This will bring us to the concept of the blockage ratio and the Krantrowitz limit. The blockage ratio is the ratio of the area available to the fluid to bypass the pod to the total cross-sectional area of the tube. It has been found by t. Kim said that no shock wave is developed for a blockage ratio of 0.25, and only a weak form of shock wave generates a blockage ratio of 0.5. thus, the blockage ratio is a single parameter that will affect all the factors in consideration, like shock wave boundary layer sensitivity and the maximum achievable velocity of the pod.

Musk's original Hyperloop proposal includes individual high-level analyses of many significant subsystems, such as the pod compression system, elevated support structure, and propulsion system. While this demon states the basic viability of the concept, it does not address significant interdisciplinary couplings inherent in the Hyperloop system. Ultimately, we need to apply a design optimization of Hyperloop to reduce construction costs, operational costs, and travel time. Performing this broader optimization is outside the scope of this work. It is reserved for future investigation since adding all of this will result in significant growth in the complexity of the Hyperloop model.

1.1. Motivation

This project is an effort to study the feasibility of Hyperloop as a fifth mode of transportation that is very

fast as well as aims to be the least expensive mode of transportation. A standard transportation system usually works in an open ambient pressure condition, so there is a lot of drag on the vehicle force while running at its cruise speed. Since Hyperloop aims to work near a vacuum or shallow pressure, much power is saved.

This project aims to design the tube that will provide the maximum velocity of the pod while keeping the other effects like shock wave, boundary layer sensitivity, and drag on the pod of hyperloop as low as possible.

1.2. Objectives

The objective of the project is: -

1. To design the tube of the Hyperloop to get the maximum speed of travel of the Hyperloop pod.
2. To minimize the effect of boundary layer sensitivity by providing sufficient bypass area.
3. To study the velocity and pressure profile during the operation of the Hyperloop.
4. To eliminate/reduce the generation of shockwaves.
5. To check the flow regimes at the time of operation.
6. Try to reduce the total drag force on the Hyperloop pod.
7. Avoid blocking or choking the bypassing air while traveling through the pod.

1.3. Background

The Hyperloop concept, introduced by Elon Musk in 2013 through the Alpha paper, proposed a high-speed transportation system using low-pressure tubes to propel capsules. SpaceX launched the Hyperloop Pod Competition in 2015 to develop subscale prototypes, with MIT's team unveiling the first scaled prototype in 2016 and demonstrating the first vacuum run in 2017. Since then, several companies in North America and Europe have been advancing Hyperloop technology for commercial use. However, deployment timelines remain uncertain as funding, regulation, and a full understanding of the system's impacts are still being addressed.

Figure 1 illustrates the worldwide presence of Hyperloop-related activities, including R&D testing facilities (green circles), completed major studies (yellow triangles), and proposed Hyperloop routes (blue diamonds). These markers span North America, Europe, Asia, and parts of the Middle East, highlighting the global interest in Hyperloop technology.

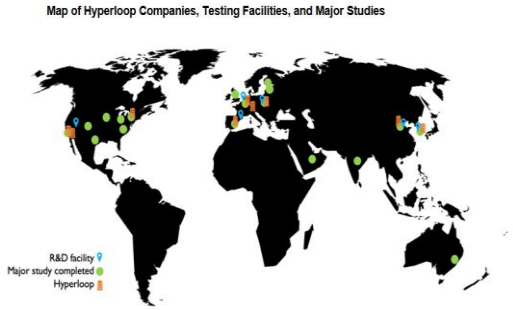

Figure 1. Global Distribution of Hyperloop Companies, testing Facilities, and major Studies [2]

2. Literature Review

This literature review examines the progress of the Hyperloop concept from its inception to its current state, drawing on 34 reports and supplemented by interviews with Hyperloop technology companies. Although Elon Musk's Alpha Paper sparked initial interest, he is no longer involved, and various firms have since refined the concept. The review highlights how some original ideas, like the elevated structure, have remained consistent while others have evolved as commercialization efforts advance. However, publicly accessible information on the pods and sensitive components is limited due to competition among developers.

Much of the available literature focuses on potential Hyperloop corridors, showcasing superior travel times, enhanced user experience, and economic benefits compared to other transport modes. Interviews with developers confirm viable solutions for critical elements such as levitation, propulsion, and guidance, but many crucial questions remain unanswered. While companies plan to license the technology, no firm investor commitments to route planning have been made yet.

2.1. Objective of Current Study

Computational fluid dynamics (CFD) is a branch of fluid mechanics that uses numerical methods and data structures to solve fluid flow problems. It relies on computers to simulate fluid interactions with surfaces under defined boundary conditions. High-speed supercomputers are often necessary for solving complex issues like transonic or turbulent flows. Continuous research enhances CFD software, improving accuracy and speed. Initial validation is typically done through wind tunnel experiments or comparison with analytical models, while full-scale testing, like flight tests, provides final validation.

CFD is widely used in aerospace, weather simulation, environmental engineering, industrial design, biological engineering, and combustion analysis. The foundation of most CFD problems lies in the Navier-Stokes equations, which describe single-phase fluid flows. These equations

can be simplified for specific scenarios, leading to the Euler or potential equations. CFD methodologies vary based on the physical assumptions of the problem, such as single-phase flow, non-reacting fluids, and whether compressibility, thermal radiation, or gravity are considered.

3. Methodology

3.1. Software Used

In this project, three software are used, namely ANSYS: This software provides a means for creating CAD files, i.e., modeling and analyzing the model under various circumstances and engineering fields. We used this software to analyze our model.

CATIA V5: - This is all-in-one software, i.e., it contains CAD, CAM, and Analysis tools. We created our model using this software.

MATLAB: - It is the renowned mathematical software that contains all the tools we come across in engineering mathematics. We plotted the conclusion graph with the help of this software.

3.2. Necessity of Considering Aerodynamic Factors Inside the Tube

The upper and lower sides of a Hyperloop pod function like converging-diverging nozzles, a well-studied scenario in wind tunnels and supersonic jet inlets. As the bypass area around the pod narrows, airflow accelerates, reaching Mach 1 at the throat (the narrowest point). If the pod's speed exceeds this, the airflow becomes choked, leading to a sharp rise in pressure drag and the formation of shock waves at the pod's tail. An increase in pressure drag will reduce the efficiency of the hyperloop system. To cure that problem, we need to pay attention to the factors which could give rise to such conditions. Figure 2 depicts a side view of an aerospace vehicle designed for Hyperloop transportation.

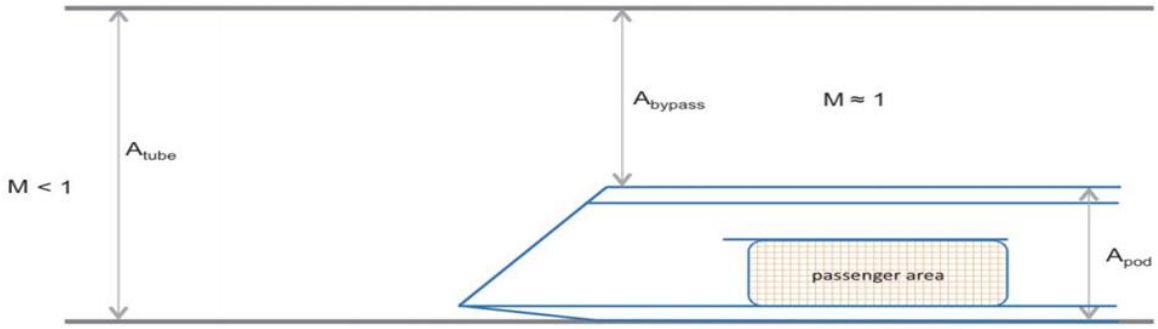

Figure 2. Schematic Representation of Hyperloop Aerodynamic Design [4]

Flow regime (or flow pattern) is information on the flow structure or flow distribution of the fluid relative to the other fluid.

This entails the flow behavior inside the hyperloop tube will change from laminar to turbulent at a particular point on the surface of the hyperloop pod.

3.4. Kantrowitz Limit

In gas dynamics, the Kantrowitz limit refers to a theoretical concept describing choked flow at supersonic or near supersonic velocities. The principle behind the Kantrowitz limit: it is the maximum amount of contraction a flow can experience before the flow chokes, and the flow speed can no longer be increased above this limit, independent of changes in upstream or downstream pressure.

For a pod traveling through a tube, the Kantrowitz limit is given as the ratio of tube area to bypass area both around the outside of the pod and through any air bypass compressor:

The given equation is plotted, and it has been seen that the area ratio increases with an increase in the pod's Mach number, but to a limit of M=1. After the sonic velocity is attained, the area ratio decreases but with a more significant slope than with which it was increasing.

$$\frac{A_{bypass}}{A_{tube}} = \left[\frac{\gamma-1}{\gamma+1}\right]^{\frac{1}{2}} \left[\frac{2\gamma}{\gamma+1}\right]^{\frac{1}{\gamma-1}} \left[1+\frac{2}{\gamma-1}\frac{1}{M^2}\right]^{\frac{1}{2}} \left[1-\frac{\gamma-1}{2\gamma}\frac{1}{M^2}\right]^{\frac{1}{\gamma-1}}$$

Where:
A_{bypass}: Fluid flow bypass area
A_{tube}: Overall tube area.
M: Mach number
$\gamma = c_p/c_v$: Isentropic expansion factor
c_p: Specific heat of fluid at constant pressure
c_v: Specific heat of fluid at constant volume

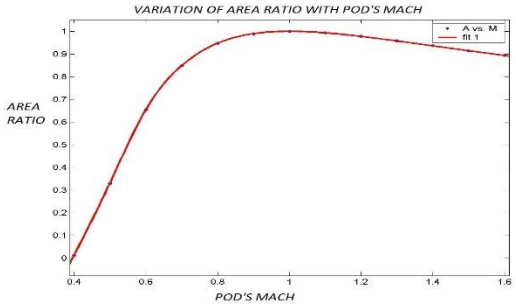

Figure 3. Kantrowitz Limit and Area Ratio [5]

The Kantrowitz limit, therefore, acts as a "speed limit" - for a given ratio of tube area and pod area, there is a maximum speed that the pod can travel before flow around the pod chokes and air resistance sharply increases. To break through the speed limit set by the Kantrowitz limit, there are two possible approaches:
The first method is to increase the tube's radial size to provide more bypass area for fluid flow around the pod, delaying the onset of choking. However, this approach is impractical as it bulges the tube and compromises system stability.

The second, more feasible method involves installing a turbine fan (compressor) at the front of the pod to draw in fluid and expel it from the rear. This reduces the fluid flowing around the pod, effectively increasing the bypass area and minimizing far-field impacts.

3.5. Boundary Layer Sensitivity

A boundary layer forms when a fluid flows over a boundary surface, where the effects of viscosity dominate.
Boundary layer formation reduces the bypass area, increasing the likelihood of flow choking. A larger tube would be required to prevent this, raising material and construction costs.
This accounts for the reduction in bypass area due to a boundary layer of arbitrary displacement thickness Since Re > 500,000, the boundary layer is assumed turbulent with a velocity profile-

$$\frac{u}{U} = (\frac{y}{\delta})^{1/7}$$

Using this boundary velocity profile, the displacement thickness of the boundary layer is derived using a similarity solution that gives the following -

$$\frac{\delta^*}{x} \approx \frac{.04775}{Re_x^{1/5}}$$

Figure 4 explores the relationship between boundary layer thickness and tube area in Hyperloop design.

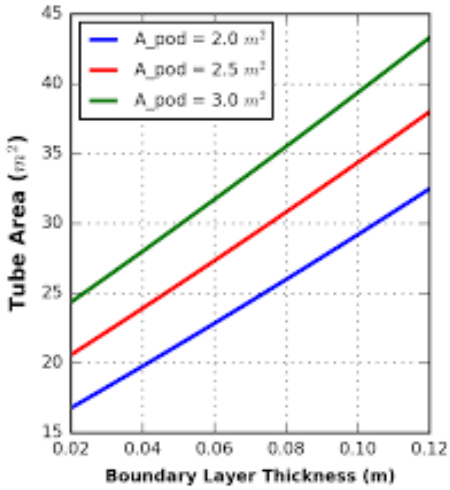

Figure 4. Boundary Layer Thickness and Tube Area [6]

Figure (b) shows the tube area variation with the pod's length. This sensitiveness is called boundary layer sensitivity. To minimize material cost, tube area and, hence, the length of the pod must be smaller. The equation and graph in Figure (b) show how sensitive the tube area is with respect to pod length. On the other hand, if we want to increase the pod passenger capacity, then instead of increasing the pod diameter (after a specific limit), an increase in the length of the pod is the better option because the rate of increase of the tube cross-sectional area also increases with pod cross-sectional area. This relationship exists because more bypass area is lost as the pod radius rises for a given displacement boundary layer thickness, so an optimum design should consider boundary layer senility and tube-pod area relation to avoid crossing the Kantrowitz limit. Figure 5 investigates the relationship between boundary layer thickness and tube area in the context of Hyperloop design.

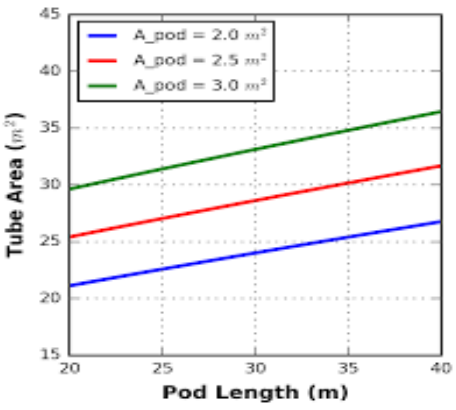

Figure 5. Kantrowitz Limit and Tube Area [7]

3.6. Remedies for Shock Wave

1. Larger tube diameter.
2. Smaller cross-sectional area for the pod.
3. Running hyperloop at lower Mach number.
4. Aerodynamic design of the nose of the pod as it will streamline the flow.
5. Bypass using compressor in pod.

3.7. Origin of Various Drag Forces in Hyperloop

1. Pressure loss due to shock waves will create wave drag (just above the pod).
2. Surface roughness (AT POD SURFACE) leads to viscous drag.
3. Boundary layer separation (AT THE END OF POD LENGTH) leads to a rise in pressure drag.

Remedies to reduce Drag

1. Roughing of nose.
2. Reduce tube pressure.
3. Removing/reducing tail.
4. Reduce the cross-sectional area of the pod.
5. Higher Reynolds number.

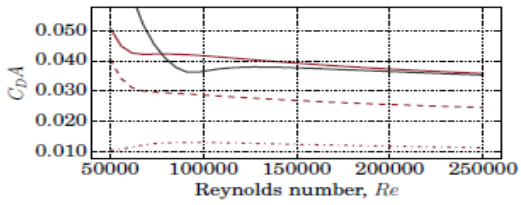

(a) Drag coefficient versus Reynolds number

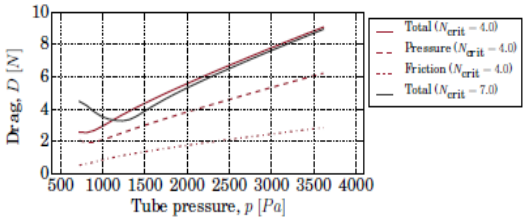

(b) Drag versus tube pressure. Note that the tube pressure is proportional to Reynolds number, because the pod velocity and tube temperature are kept constant here.

Figure 6 (a): Drag Coefficient versus Reynolds Number and (b) Drag versus Tube Pressure [7]

Drag force decreases as the tube pressure is decreased. This is because the value of skin friction drags decreases because of a reduction in rubbing action between the fluid flow and the pod. As the value of the Reynolds number increases, the flow becomes turbulent. It has been found that turbulence flow can delay the boundary layer separation much better than the laminar flow and will ultimately reduce the wave drag on the pod.

4. Results and Discussions

4.1. Specifications

- Pod diameter = 2.23m
- Pod length = 10m
- Tube length = 30m
- Pod shape – Article by Yadawendra Singh and Kamyar Mehran [7]
- Air pressure inside tube = 100 Pa
- Pod speed = 900km/hr (250 m/s) and
- based on sound velocity 343m/s, Mpod = 0.72886

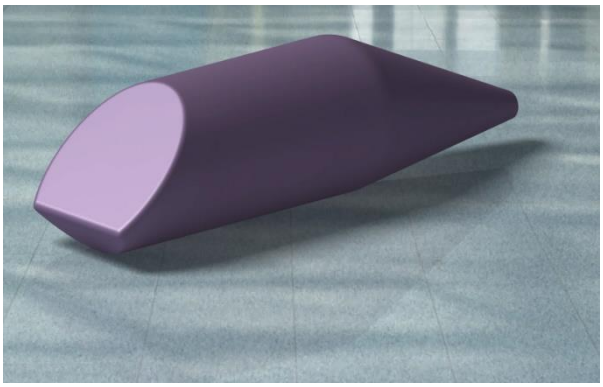

Figure 7. Hyperloop cad model of tube pod

4.2. Meshing

Mesh size – 50mm

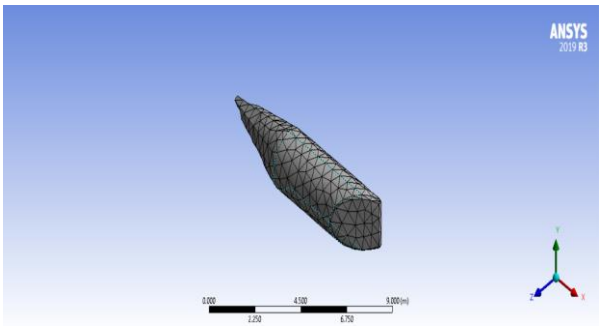

Figure 8. 3D mesh model of a Hyperloop tube pod

Figure 9. 3D mesh model of outer tube

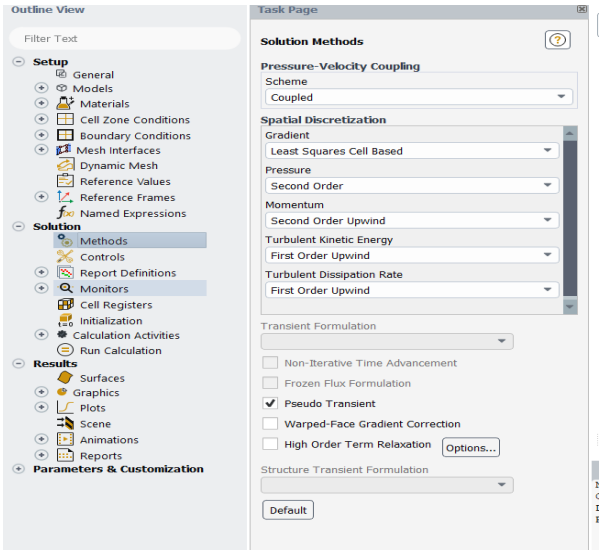

Figure 10. Screenshot from a simulation software interface

4.3. Boundary Conditions

- Inlet speed – 250m/s
- Tube inside pressure – 100Pa
- Pod and Tube wall – No slip condition

4.4. Tube diameter – 9.735m

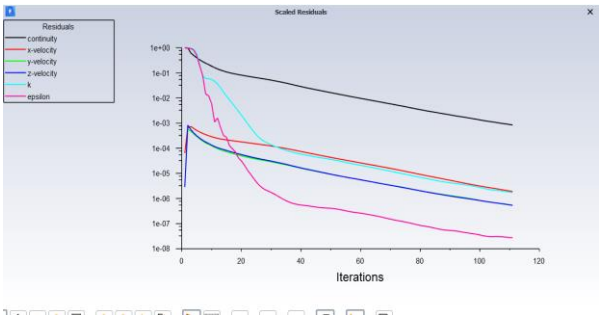

Figure 11. performance of a model over iterations

Figure 12 presents a detailed computational analysis of a Hyperloop pod within its outer tube. The model uses ANSYS software to display the stress distribution across the pod and tube vividly. The color gradient, ranging from blue (low stress) to red (high stress), visually represents the structural stresses encountered under simulated conditions. Notably, the green outer tube exhibits varying shades to indicate stress levels, while the pod's interior stresses are similarly color-coded. A sectional view permits an in-depth examination of the internal components, which is crucial for assessing the design's integrity and performance. The accompanying color scale and axes ensure precise stress values and orientation interpretation. This analysis is pivotal for optimizing the Hyperloop's design for safety and efficiency in high-speed transit applications.

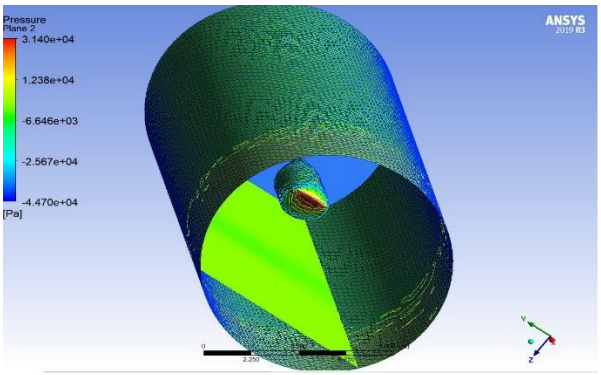

Figure 12. Stress Distribution Analysis of a Hyperloop Pod within an Outer Tube Using ANSYS

Figure 13 depicts a computational fluid dynamics simulation that analyzes the velocity magnitude of fluid flow within a pipe. The simulation using ANSYS software employs a color scale to represent velocity magnitudes, with red and orange highlighting areas of higher velocities. The green pipe and its internal structure are color-coded to indicate different velocity zones, aiding in identifying potential flow irregularities and optimizations. The color scale ranges from 0.000e+00 to 3.576e-02 m/s, precisely quantifying the flow velocities. This analysis is essential for optimizing fluid dynamics within the pipe system, ensuring efficient flow, and minimizing turbulence-related issues. The 3D model orientation is denoted by the labeled axes at the bottom right corner, ensuring accurate spatial interpretation. This detailed visualization is a critical tool for engineers in designing and analyzing fluid systems.

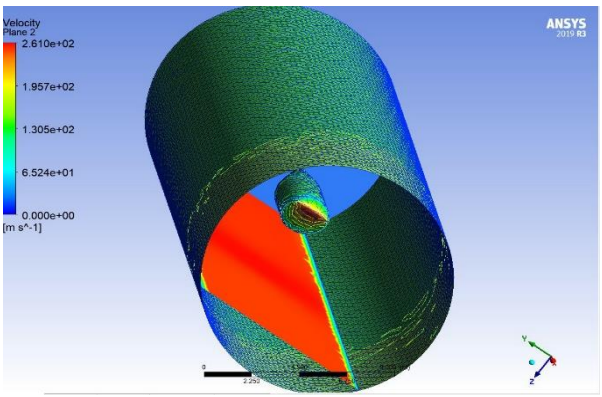

Figure 13. Velocity Magnitude Analysis in a Pipe Using Computational Fluid Dynamics

4.5. Tube diameter – 7m

Figure 14 showcases a graphical analysis of various parameters over 100 iterations as part of an optimization process in a computational model. The graph displays multiple lines, each representing a different parameter such as sensitivity, specificity, positive predictive value, negative predictive value, and accuracy. These parameters are plotted against the

'Bucket bandwidth' on a logarithmic scale, illustrating their evolution and optimization over the course of the iterations. The lines begin at higher values and exhibit a decreasing trend, signifying the refinement and learning process inherent to the model's design. This visualization is instrumental in understanding the dynamics of the model's performance and guiding further enhancements. The clear demarcation of iterations and bucket bandwidth values, along with the distinct color coding for each parameter, facilitates an intuitive interpretation of the model's behavior over time.

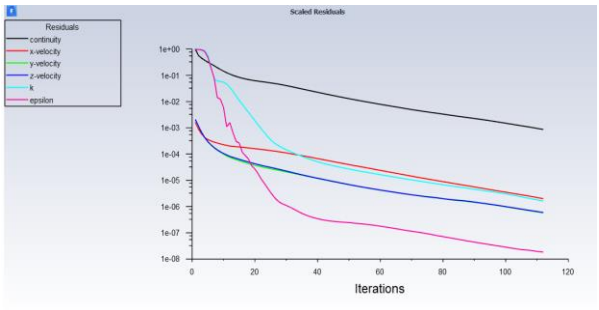

Figure 14. Optimization of Parameters Over Iterations in a Computational Model

Figure 15 illustrates a computational simulation that visualizes the pressure distribution on an aerodynamic shape resembling an airfoil. The simulation, likely conducted using software such as ANSYS, employs a color-coded legend to denote pressure levels, with the spectrum ranging from -2.77e+04 to 7.77e+04. The 3D model at the center is rendered with corresponding colors to indicate varying pressure zones, which is critical for analyzing aerodynamic performance. Adjacent outlined shapes may represent alternative viewing angles or related simulations, providing a comprehensive understanding of the pressure effects. A scale bar and coordinate system axes (XYZ) at the bottom center ensures accurate spatial interpretation of the model. This simulation is pivotal for optimizing the design and performance of aerodynamic structures in various engineering applications.

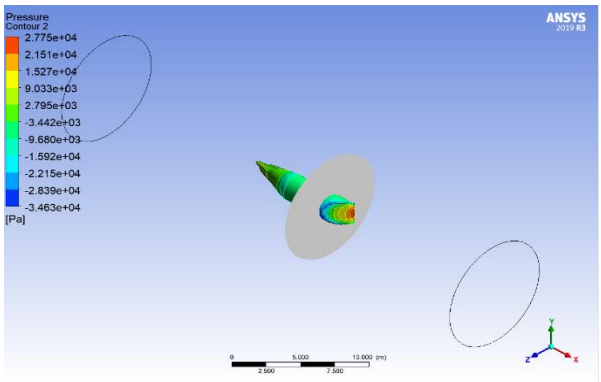

Figure 15. Pressure Distribution on an Aerodynamic Shape in a Computational Simulation

Figure 16 exhibits a computational simulation of the velocity field surrounding a high-speed object akin to a bullet or an airfoil. The simulation, likely conducted using ANSYS software, features a color scale delineating velocity values from 0.000e+00 (indicating stationary) to 3.500e+02 (indicating high velocity). The object is depicted in blue, signifying its rapid movement from left to right. At the same time, the surrounding flow field is represented by a spectrum of colors corresponding to various velocities. This visualization is crucial for analyzing the aerodynamic properties of the object and optimizing its design for superior performance in high-speed environments. The scale bar and coordinate system indicators at the bottom provide a reference for scale and orientation, enhancing the accuracy of the analysis. This detailed simulation serves as an invaluable tool for engineers focusing on the dynamics of high-speed motion and fluid interactions.

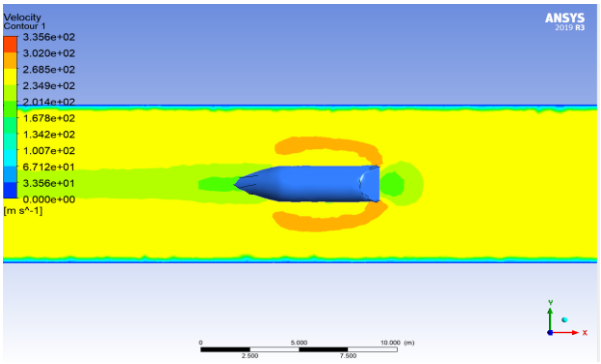

Figure 16. Velocity Field Simulation around a High-Speed Object

4.6. Tube diameter – 4m

Figure 17 provides a comparative analysis of the impact of different actor learning rates on the total reward in a reinforcement learning model. The graph plots the evolution of the total reward over 140 iterations, with five distinct lines representing actor learning rates ranging from 0.0003 to 0.007. Each line, color-coded for clarity, demonstrates the learning process and optimization of the model as it interacts with the environment. The trend observed across the iterations suggests a significant influence of the actor learning rate on the model's performance, with some rates leading to better convergence than others. This analysis is crucial for fine-tuning the learning parameters to achieve optimal results in complex adaptive systems. The legend in the top left corner correlates the colors to the respective learning rates, ensuring a clear understanding of the data presented.

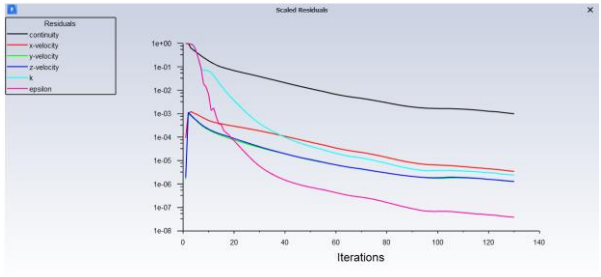

Figure 17. Comparative Analysis of Actor Learning Rates in Reinforcement Learning

Figure 18 demonstrates a computational fluid dynamics simulation that maps pressure contours onto an aerodynamic model, potentially an airfoil. The simulation, likely performed using ANSYS software, features a color gradient to represent pressure levels from 2.077e+04 to -5.000e+04 [Pa]. The central object is detailed with these contours, providing insights into pressure distribution critical for aerodynamic analysis. The two circular outlines adjacent to the model may offer additional perspectives or relate to comparative studies. The Cartesian coordinate system at the bottom right ensures accurate orientation, while the gradient blue background enhances the visual appeal of the simulation. This analysis is key for optimizing aerodynamic designs and improving performance in fluid dynamic environments.

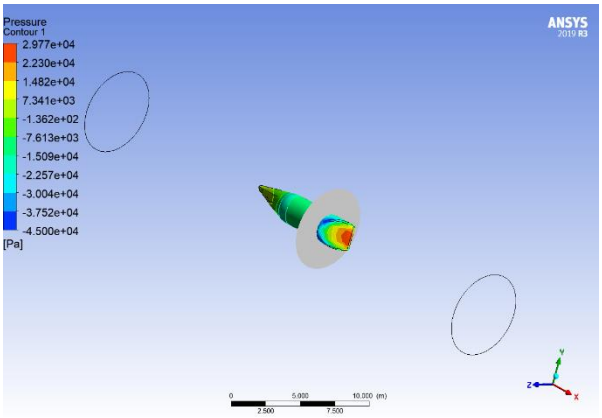

Figure 18. Pressure Contour Analysis on an Aerodynamic Model

Figure 19 displays a computational fluid dynamics simulation that analyzes the velocity distribution around an aerodynamic cone model. The simulation, likely performed using ANSYS software, utilizes a color scale to indicate velocity values from 0 to 3.47e+02 m/s. The model is centrally placed and color-coded to reflect the varying velocities, which are essential for studying the object's aerodynamic properties. The outlined ellipses may represent different flow patterns or comparative analyses. The inclusion of a scale bar and XYZ axis indicator at the bottom provides a reference for orientation and scale. This simulation is vital for understanding the fluid dynamics around high-speed objects and optimizing their design for improved performance in aerospace applications.

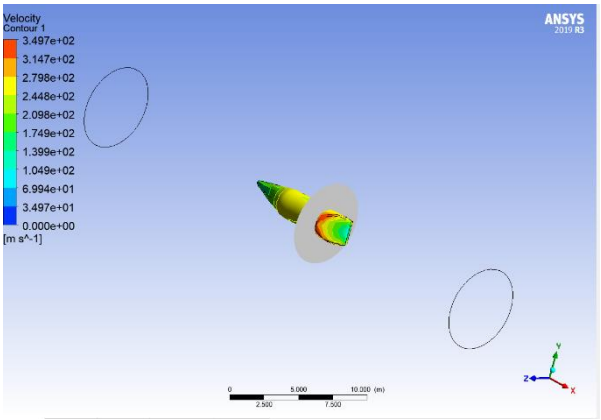

Figure 19. Velocity Distribution Analysis on an Aerodynamic Cone Model

Figure 20 illustrates the relationship between tube diameter and system performance, as a simple line graph indicates. The x-axis represents the tube diameter, ranging from 0 to 11, while the y-axis, though not labeled, shows values that suggest a performance metric ranging from 4.0 to 5.2. The graph plots three data points connected by a blue line, indicating a trend where performance peaks at a tube diameter of 3 and gradually decreases as the diameter increases. This analysis is crucial for optimizing tube dimensions to achieve the best system performance in fluid dynamics or heat transfer systems applications. The graph provides a clear visual representation of how changes in physical dimensions can affect a mechanical system's overall efficiency and effectiveness.

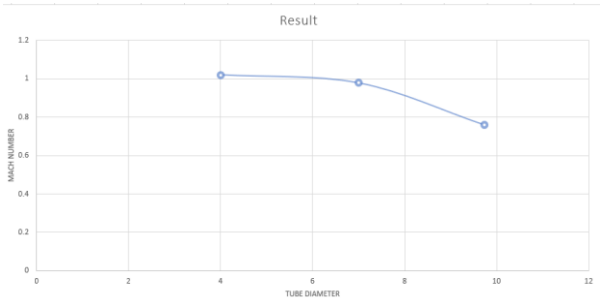

Figure 20. Impact of Tube Diameter on System Performance

Figure 21 presents a trend analysis graph labeled "Kontrolle Limit," which examines the progression of control limits across different tube diameters. The x-axis, now representing "Tube Diameter," spans from 0 to 10, while the y-axis, though not explicitly labeled, ranges from 0 to 10, likely indicating control limit values. The

graph plots five data points connected by a blue line that exhibits a gradual increase, suggesting an upward trend in control limits as the tube diameter increases. This visualization aids in monitoring and managing quality control parameters, ensuring that the system remains within the defined control limits for optimal performance. The simple yet informative graph provides a clear view of the relationship between tube diameters and control limits, which is essential for process optimization and management.

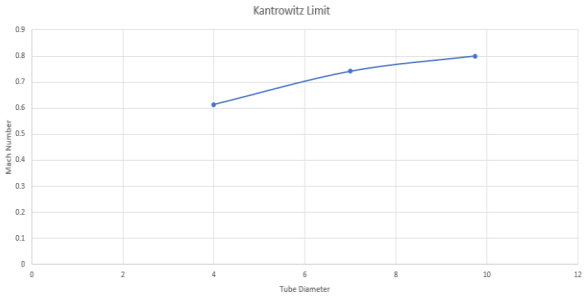

Figure 21: Trend Analysis of Control Limits Over Varying Tube Diameters

5. Conclusion

In our analysis of different tube diameters for the hyperloop pod system, we have found that a diameter of approximately 7 meters is optimal for our pod geometry. This diameter minimizes the bypass air speed, keeping the Mach number below 1, which is crucial for safety and efficiency. Comparing diameters of 9.735 meters, 7 meters, and 4 meters, we observed significant differences in various factors such as choke flow occurrence, shock wave generation, boundary layer effects, material requirements, compressor work, stability, and future scopes for improvement. For future enhancements, several avenues can be explored including the utilization of advanced alloy materials, adjustments in tube thickness to mitigate buckling, optimization of column spacing and cross-section, utilization of compressors for bypass air management, exploration of different column lengths and cross-sectional shapes, implementation of turbulence-generating techniques, and thorough investigation into the effects of tail variations on pod performance.

Furthermore, considering underwater structures presents intriguing possibilities, offering advantages such as reduced weight, inherent damping properties, adjustable pressure maintenance, and simplified route design, particularly in urban settings. These insights provide a robust foundation for further research and development in the realm of hyperloop transportation systems.

References

[1] www.wikipedia.com

[2] www.sciencedirect.com

[3] www.google.com

[4] www.skybrary.aero

[5] Open-Source Conceptual Sizing Models for The Hyperloop Passenger Pod Jeffrey C. Chin∗, Justin S. Gray∗, Scott M. Jones∗, Jeffrey J. Berton∗ Nasa Glenn Research Center, Cleveland, Oh

[6] X International Conference On Structural Dynamics, Eurodyn 2017 Transpod Ultra-High-Speed Tube Transportation Ryan Janzen.

[7] "Mit Hyperloop Final Report" An Overview Of The Design, Build,And Testing Process For Mit's Entry In The Spacex Hyperloop Competition 2015-2017 August 2017 Cleared For Public Release ©Mit Hyperloop Team 2017.

[8] "Hyperloop Alpha" Elon Musk 2013 Research Paper.

[9] "Conceptual Feasibility Study of Hyperloop Vehicle" By Nasa Glenn Research Center, Cleveland, Oh.

[10] Hyperloop Technology: Economic Analysis of a Transportation Revolution "Jacob Covell"

BIOGRAPHIES

Mr. Rahul Sahu is an Assistant Professor at GEC Raipur. He did his MTech from IIT Bombay and is pursuing PhD from IIT Bhilai.

Mrs. Swastika Patel is an Assistant Professor at GEC Raipur. She did her MTech from NERIST Itanagar and pursuing PhD from IIT Bhilai.

Mr. Prashant Kumar Sahu is an Assistant Professor at GEC Jagdalpur. He did his MTech from IIT Guwahati and pursuing PhD from CSVTU Bhilai.

Mr. Gulab Verma is an Assistant Professor at GEC Jagdalpur. He did his MTech from NIT Suratkal and pursuing PhD from NIT Raipur.

Mr. Sunil Kumar Patel is an Assistant Professor at GEC Raipur. He did his MTech from MNIT Bhopal.